Modeling Water Vapor and Clouds as Passive Tracers in an Idealized GCM

YI MING AND ISAAC M. HELD

NOAA/Geophysical Fluid Dynamics Laboratory, Princeton, New Jersey

(Manuscript received 15 November 2016, in final form 10 May 2017)

ABSTRACT

This paper introduces an idealized general circulation model (GCM) in which water vapor and clouds are tracked as tracers, but are not allowed to affect circulation through either latent heat release or cloud radiative effects. The cloud scheme includes an explicit treatment of cloud microphysics and diagnoses cloud fraction from a prescribed subgrid distribution of total water. The model is capable of qualitatively capturing many large-scale features of water vapor and cloud distributions outside of the boundary layer and deep tropics. The subtropical dry zones, midlatitude storm tracks, and upper-tropospheric cirrus are simulated reasonably well. The inclusion of cloud microphysics (namely rain re-evaporation) has a modest but significant effect of moistening the lower troposphere in this model. When being subjected to a uniform fractional increase of saturated water vapor pressure, the model produces little change in cloud fraction. A more realistic perturbation, which considers the nonlinearity of the Clausius–Clapeyron relation and spatial structure of CO_2-induced warming, results in a substantial reduction in the free-tropospheric cloud fraction. This is reconciled with an increase of relative humidity by analyzing the probability distributions of both quantities, and may help explain partly similar decreases in cloud fraction in full GCMs. The model provides a means to isolate individual processes or model components for studying their influences on cloud simulation in the extratropical free troposphere.

1. Introduction

A complicating factor in simulating and understanding the climatic roles of water vapor (WV) and clouds is their tight coupling with circulation, posing a major bottleneck in narrowing the uncertainty of cloud feedback (Bony et al. 2015). This motivates us to construct a model of passive WV and clouds, meaning that both are advected as tracers that do not feed back on circulation either through latent heat release or through cloud radiative effects (CRE). Such a model can be thought of as part of a model hierarchy designed for elucidating the complex interplay between moisture and circulation (Held 2005). In particular, it would be complementary to a class of widely used idealized models that consider latent heat release but do not allow large-scale cloud formation explicitly (Frierson et al. 2006; Frierson 2007; O'Gorman and Schneider 2008).

Besides cloud feedback, this model may help address what factors have the potential to control the large-scale distribution of tropospheric WV. Sun and Lindzen (1993) postulated that tropical relative humidity (RH) was influenced significantly by cloud microphysics, in particular re-evaporation of hydrometeors. This view was later countered by a body of literature collectively known as the advection–condensation theory (Sherwood 1996; Salathé and Hartmann 1997; Pierrehumbert et al. 2007, and references therein), which put more emphasis on circulation and succeeded in reproducing some gross features of RH. These studies typically used simple saturation adjustment (i.e., WV in excess of saturation being removed instantaneously as surface precipitation) and did not include explicit cloud microphysics. Models with passive WV and clouds would allow us to re-evaluate the relative importance of cloud microphysics and circulation in setting tropospheric RH in a self-consistent framework.

In the context of a model in which water vapor and clouds are passive, designing sensitivity experiments in such a way as to mimic global warming simulations is difficult. This issue is best exemplified by the "fixed anvil temperature hypothesis" (Hartmann and Larson 2002), which argues that the temperature of the upper-level

Denotes content that is immediately available upon publication as open access.

Corresponding author: Yi Ming, yi.ming@noaa.gov

Publisher's Note: This article was revised on 15 January 2018 to include the open access designation that was missing when originally published.

DOI: 10.1175/JCLI-D-16-0812.1

outflow generated by tropical convection will not change appreciably in response to warming despite the increase in upper-level temperatures, due to upward extension of the convection. Without this vertical expansion of the convection, warming of the tropics will, for example, favor increasing RH throughout the subtropics, an effect not seen in GCMs in which the circulation and the WV and cloud fields interact. While this vertical expansion of the troposphere can affect the midlatitudes as well, our hope is that there are aspects of the relative humidity and clouds in midlatitudes that are not so tightly tied to interactions with the circulations so that analysis of a passive model will be of value.

The main purpose of this paper is to document the model formulation and main characteristics of control simulations, starting a conversation on the role a model of this type might play in analyzing RH and cloud fields. A secondary purpose is to use a set of perturbation experiments to substantiate the model's utility in studying, in isolation, key processes underlying cloud feedback. Although the large-scale distribution of WV has been studied extensively with idealized models of different kinds (e.g., Galewsky et al. 2005; Sherwood and Meyer 2006), it is still unclear whether insights developed for WV are applicable to clouds. In this paper, we choose to discuss both water vapor and clouds as the former is a natural starting point for thinking about the latter. Although it is reassuring that some of our results with respect to WV are broadly consistent with the previous studies, the novelty of this work lies mostly in the cloud part.

2. Model description and experimental design

The model described here is an example of a class of models that can be constructed based on an atmospheric dry dynamical core coupled with a GCM's cloud physics, or with more simplified or more complex versions of the latter. There is no convective parameterization. The large-scale flow is unaffected by the WV and cloud fields. In theory the flow could be stored offline and read into the model as needed but this is typically inconvenient.

Our example of such a model (referred to as the cloud model here) is forced thermally to a prescribed equilibrium temperature profile via Newtonian relaxation, and, as there is no explicit boundary layer parameterization, wind fields are damped by Rayleigh friction near the surface, precisely as in Held and Suarez (1994). Three water tracers are advected: specific humidity, liquid, and ice condensates. Surface evaporation is mimicked by nudging RH below ~850 hPa to 100% with a time scale of 30 min. The large-scale cloud scheme is the same as implemented in the Geophysical Fluid Dynamics Laboratory (GFDL) HiRAM (Zhao et al. 2009). Cloud fraction and condensation are diagnosed from grid-mean total water (WV and cloud condensates) using an assumed subgrid-scale distribution, which takes the form of a beta distribution with the width controlled by the grid-mean total water multiplied by a width parameter, just as in Tompkins (2002). The shape parameters p and q in Eq. (7) of Tompkins (2002) are set at 5, resulting in a symmetrical distribution; the width parameter is set at 0.2 in our control simulation. Cloud microphysics is adopted from Rotstayn (1997) and Rotstayn et al. (2000), as in the atmospheric component of GFDL CM2 (AM2; Anderson et al. 2004) and the atmospheric component of GFDL CM3 (AM3; Donner et al. 2010). This single-moment scheme takes into account the main pathways for transformation between cloud condensates, precipitation formation, and re-evaporation of condensates and precipitation. Condensation (re-evaporation) is assumed not to generate latent heating (cooling) and thus does not affect flow. There are no cloud or WV radiative effects as no explicit radiation is involved. In this sense, WV and clouds are completely passive. Using the cloud scheme from a particular full GCM in this way is a test of concept. Examining a whole variety of microphysical schemes may be of interest in this context, varying from much more idealized schemes, to the schemes used in other GCMs, to bin-microphysical models. One could also potentially compute radiative fluxes and heating rates implied by the WV and cloud distributions, using full radiative transfer codes, but not interacting with the flow, as an offline measure of sensitivity to different microphysical modules.

The model analyzed here has a spectral dynamical core with a horizontal resolution of T42, and 20 equally spaced vertical sigma layers. There is no claim that this simulation is converged as horizontal and especially vertical resolution is increased. Studies of the dependence of results such as these on resolution, and the dynamical core more generally, will hopefully be facilitated by this model configuration. The algorithm for tracer advection is identical to that used for passive tracer advection with this spectral dynamical core in the past (e.g., Galewsky et al. 2005; Polvani and Esler 2007). Since it has not been documented in those studies, we describe it in a short appendix.

In an alternative model configuration (referred to as the saturation adjustment model), the cloud scheme is replaced with saturation adjustment. The only water tracer is specific humidity. As any newly formed condensate is assumed to fall out of the air immediately, this model, which is similar to that used in Galewsky et al. (2005), cannot be used to simulate clouds, although one can compute the fraction of time that the air at a particular location is saturated, a diagnostic that may be helpful in understanding cloud changes in models with

explicit condensate. We perform control simulations with these two models (referred to as CNTL-C and CNTL-SA, respectively). The RH difference between them tells us how the inclusion of the cloud scheme influences the distribution of tropospheric WV. To further separate the influences of cloud macrophysics (partial cloudiness in the cloud model vs full cloudiness in the saturation adjustment model) and microphysics (present in the cloud model vs absent from the saturation adjustment model), we design a sensitivity experiment with the cloud model, in which the aforementioned width parameter is lowered to 0.01. This has an effect of allowing for cloud formation only when grid-mean RH essentially reaches 100%, thus switching from zero to full cloudiness, and represents a straightforward way to mimic saturation adjustment in the cloud model. This experiment is referred to as NW (for narrower width). The difference between CNTL-C and NW can be attributed to the change of cloud macrophysics, while the inclusion of cloud microphysics results in the difference between NW and CNTL-SA.

To explore the responses of WV and clouds to increased saturated water vapor pressure e_s, we carry out three perturbation experiments with the default cloud model. In the first one (referred to as UN, for uniform), the e_s term used in moist physics and diagnosis (e.g., RH) (denoted as e_s^*) is increased uniformly by 14%, regardless of temperature T:

$$e_s^*(T) = 1.14 e_s(T). \tag{1}$$

This is motivated by the commonly held notion that e_s increases with T approximately by $7\%\,\mathrm{K}^{-1}$, a useful starting point for thinking about the hydrological response to CO_2-induced warming. In this sense, the specified e_s increase represents the thermodynamical effect of a 2-K warming. This, however, is strictly valid only for a temperature range typical of the surface. The second experiment (referred to as TS, for temperature squared) relaxes this restriction by taking into account the temperature dependence of the Clausius–Clapeyron relation:

$$e_s^*(T) = 1.14 e_s(T)\left(\frac{293}{T}\right)^2. \tag{2}$$

At 233 K (representative of the upper troposphere), the percentage increase is about 80%, much larger than at the surface. In the third experiment (referred to as TC, for temperature cubed), we further enhance the temperature dependence from square to cubic to partially factor in the effect of upper-tropospheric amplification, a consequence of the moist adiabatic lapse rate, as well as polar amplification. The resulting expression is

TABLE 1. Summary of the experiments.

Name	Description
CNTL-SA	Control simulation with saturation adjustment
CNTL-C	Control simulation with the cloud scheme
NW	Based on CNTL-C, but with a smaller width parameter
UN	Based on CNTL-C, but with a uniform increase of e_s
TS	Based on CNTL-C, but with an increase of e_s inversely proportional to T^2
TC	Based on CNTL-C, but with an increase of e_s inversely proportional to T^3

$$e_s^*(T) = 1.14 e_s(T)\left(\frac{293}{T}\right)^3. \tag{3}$$

This further elevates the percentage increase to about 130% for 233 K. For a surface warming of 2 K, the upper troposphere can be warmer by 5 K in GCMs, which would increase local e_s by about 200%. Therefore, the cubic dependence still likely underestimates the relative change of e_s for the upper troposphere.

In using this procedure to mimic some of the effects of warming, one must keep in mind the several ways in which this cannot capture the effects of warming in comprehensive models. These include the effects of changes in circulation and also the effects of warming on the ice/liquid partitioning in clouds. Thus, the perturbation experiments should not be interpreted as directly comparable to full GCM warming experiments. One can refer to Table 1 for a summary of the various experiments.

3. Results

a. Control simulations

A measure of the overall hydrological cycle strength, the global-mean precipitation (evaporation) is virtually the same ($\sim 2.4\,\mathrm{mm\,day}^{-1}$) in CNTL-C and CNTL-SA. Except for small differences in the deep tropics and mid- to high latitudes, the zonal distributions of precipitation and evaporation are also similar (Fig. 1). The precipitation features three distinct peaks in the deep tropics and over the midlatitude storm tracks, and is outweighed by evaporation by a factor of 4–5 in the subtropical dry zones. These results confirm that detailed cloud microphysical treatment is not necessary for simulating the large-scale features of the hydrological cycle in these passive models. This does not necessarily imply that the precipitation distribution is unaffected by cloud microphysical assumptions in comprehensive GCMs due to at least two complicating factors. First, the

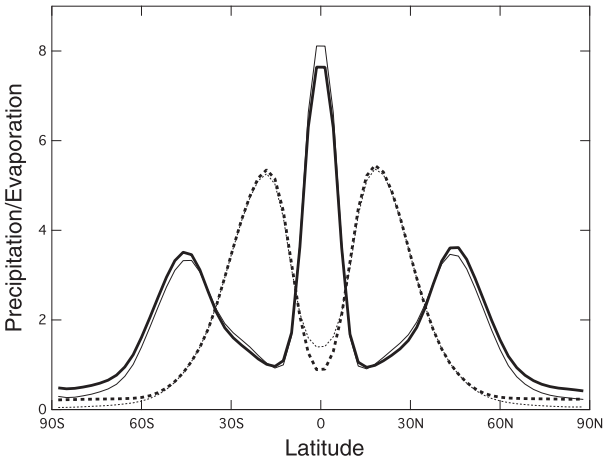

FIG. 1. Zonal-mean precipitation (mm day^{-1}; solid lines) and evaporation (mm day^{-1}; dotted lines) simulated in CNTL-C (thick lines) and CNTL-SA (thin lines).

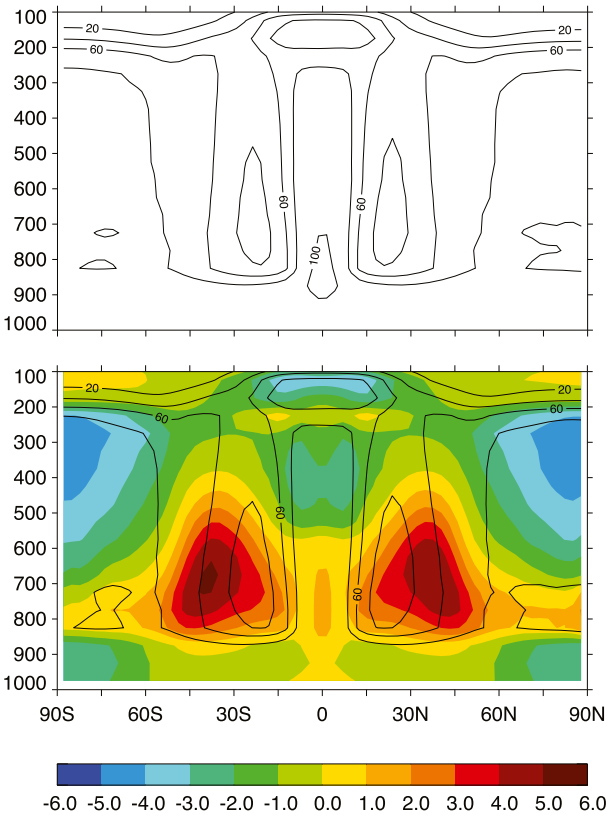

FIG. 2. RH (%; contours with an interval of 20%) simulated in (top) CNTL-C and (bottom) CNTL-SA. The difference (defined as the former minus the latter throughout this paper) is shown in color shading in bottom.

flow field in the passive models does not vary with cloud microphysics by design. Second, the hydrological cycle in comprehensive GCMs is constrained by the atmospheric radiative balance, while there exists no such constraint in these passive models. In these models, the strength of the hydrological cycle is controlled by the rate of export of WV out of the saturated boundary layer by the circulation. This is true in more comprehensive models as well, but there is no feedback here between the radiative cooling of the free troposphere with the circulation exporting WV out of the boundary layer.

A comparison with the aquaplanet simulations performed with the comprehensive GCMs in the Aquaplanet Intercomparison Project [Fig. 3 of Blackburn et al. (2013)] suggests that the cloud model captures many gross features of the global RH distribution, including the subtropical dry zones, dry upper troposphere, and moist mid- and high latitudes. The RH in the deep tropics (15°S–15°N) is too high (over 80%) due to the absence of moist convection either parameterized or resolved, which is the main mechanism of tropical dehydration in comprehensive GCMs. For the same reason, the outflow from the tropical ascent is more spread vertically in this model than in the aquaplanet simulations, causing the subtropical dry zones to be placed lower. Similar conclusions can be drawn by comparing with the comprehensive model results from phase 3 of the Coupled Model Intercomparison Project [Fig. 1 of Sherwood et al. (2010)]. Replacing saturation adjustment with the cloud scheme tends to moisten the subtropics and midlatitudes (15°–60°) by a few percent (in absolute RH) (Fig. 2, bottom). The drying of the polar upper troposphere can be attributed partly to the treatment of partial cloudiness in the cloud model as described below.

The total nonevaporation WV tendency is given in Fig. 3. The three local maxima (the deep tropics and midlatitudes) correspond to the intertropical convergence zone (ITCZ) and storm tracks (Fig. 3, top). Both models generate similar spatial patterns, substantiating that saturation adjustment, as simple as it is, is indeed sufficient for capturing the gross features of precipitation. The biggest differences lie approximately over ~30°–60° and between ~500 and 800 hPa; the WV sink (or the condensate source) is stronger in CNTL-C than in CNTL-SA, coinciding with higher surface precipitation associated with storm tracks in the former.

Needless to say, condensation is the dominant sink of WV, but it is of interest to examine the other secondary terms (Fig. 4). Ice deposition takes over in the upper troposphere but is about one order of magnitude smaller than condensation. Rain re-evaporation, which occurs when falling raindrops enter unsaturated air, is a non-negligible source of WV in the subtropical and midlatitude lower troposphere. A sensitivity experiment with re-evaporation switched off indicates that it is indeed partly responsible for the moistening. (In comparison,

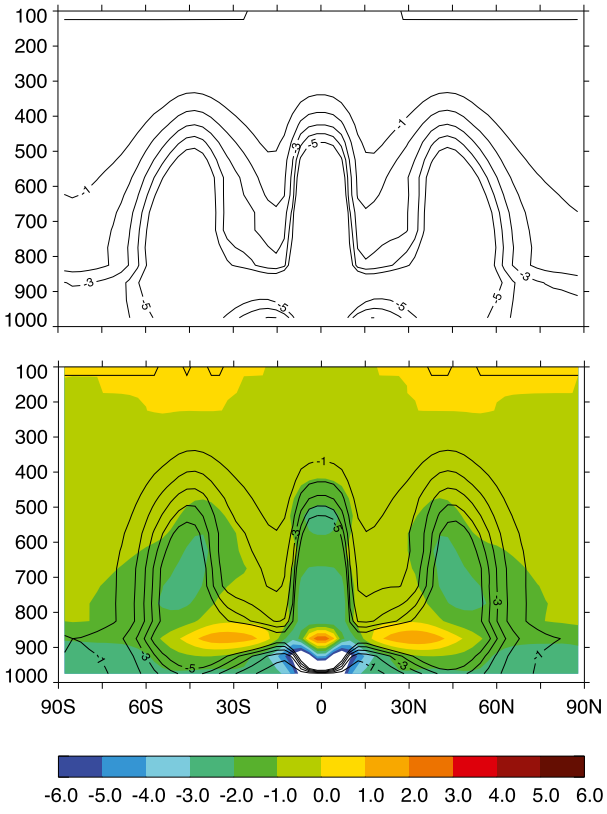

FIG. 3. Total WV tendency due to phase transition (not including evaporation) (10^{-9} kg kg^{-1} s^{-1}; contours with an interval of 1×10^{-9} kg kg^{-1} s^{-1}) in (top) CNTL-C and (bottom) CNTL-SA. The difference is shown in color shading in bottom. White in a colored figure indicates that values are outside the range of the color bar throughout the paper.

cloud liquid re-evaporation is almost negligible, and is not shown.) As another source of WV over the midlatitudes, snow sublimation is of comparable magnitude but generally deeper into the atmosphere's interior than re-evaporation.

As described in the previous section, NW is an intermediate case between CNTL-C and CNTL-SA. Figure 5 (top) shows that the consideration of partial cloudiness tends to decrease simulated RH everywhere by allowing cloud and precipitation to form at a lower RH threshold value. The largest reduction (more than 3%) occurs over the high latitudes, indicating that the different treatment of subgrid variability is responsible for a similar feature of the RH difference between the two control simulations (Fig. 2, bottom). The effect of incorporating cloud microphysics can be isolated by comparing NW with CNTL-SA (Fig. 5, bottom). It has marked spatial structure, with significant moistening in the lower troposphere (especially over ~15°–60°), which is also present in the RH difference between CNTL-C and CNTL-SA. This confirms the significant role of microphysics in modifying

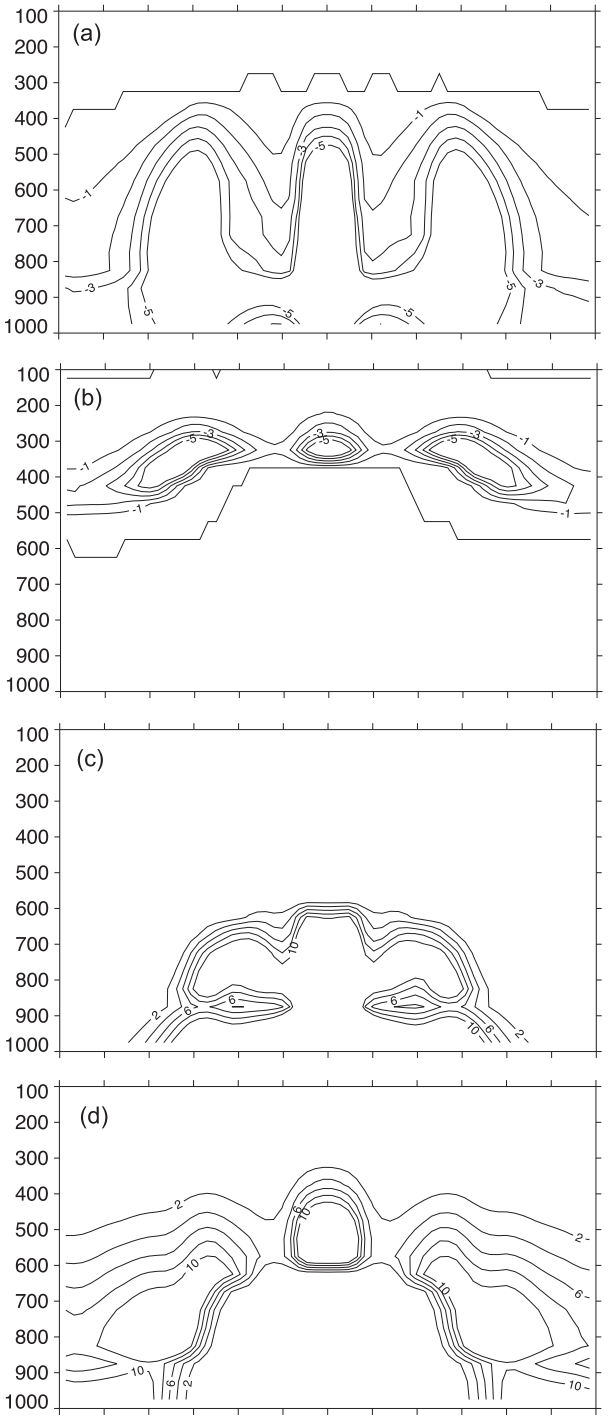

FIG. 4. WV tendencies due to (a) condensation (10^{-9} kg kg^{-1} s^{-1}; contours with an interval of 1×10^{-9} kg kg^{-1} s^{-1}), (b) ice deposition (10^{-10} kg kg^{-1} s^{-1}; contours with an interval of 1×10^{-10} kg kg^{-1} s^{-1}), (c) rain re-evaporation (10^{-10} kg kg^{-1} s^{-1}; contours with an interval of 2×10^{-10} kg kg^{-1} s^{-1}), and (d) snow sublimation (10^{-10} kg kg^{-1} s^{-1}; contours with an interval of 2×10^{-10} kg kg^{-1} s^{-1}) in CNTL-C. Cloud liquid re-evaporation and ice sublimation are negligible.

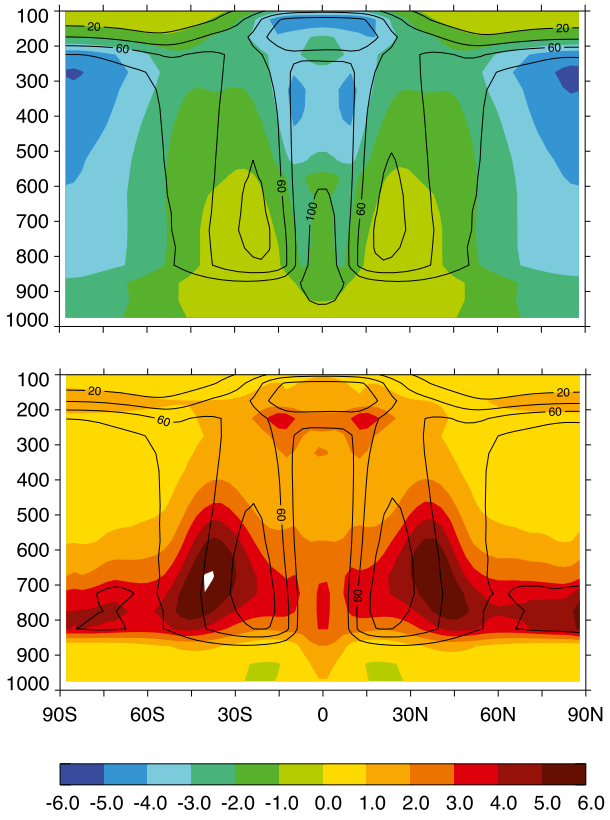

FIG. 5. RH difference (%; color shading) between (top) CNTL-C and NW and (bottom) NW and CNTL-SA (color shading). The contours with an interval of 20% represent RH in NW and in CNTL-SA in the top and bottom, respectively.

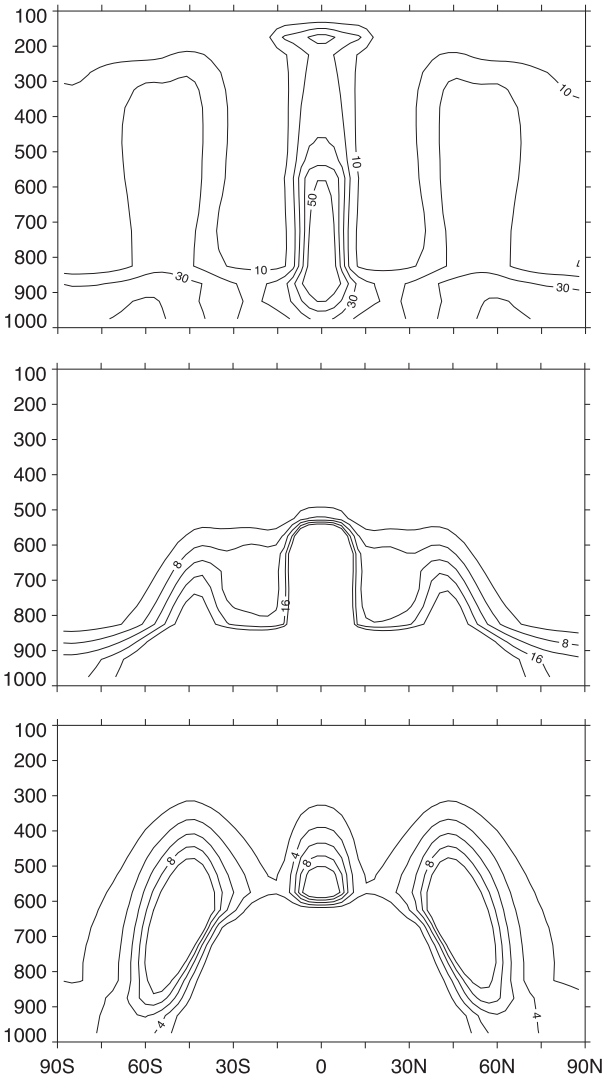

FIG. 6. (top) Cloud fraction (%; contours with an interval of 10%), (middle) liquid (10^{-6} kg kg^{-1}; contours with an interval of 4×10^{-6} kg kg^{-1}), and (bottom) ice (10^{-6} kg kg^{-1}; contours with an interval of 2×10^{-6} kg kg^{-1}) in CNTL-C.

lower-tropospheric RH in this model (Wright et al. 2009; Sherwood and Meyer 2006).

Figure 6 depicts the simulated cloud fields in CNTL-C. The simulated boundary layer clouds are unrealistic due to the lack of a boundary layer scheme, and we view this model's relevance as restricted to the free troposphere. The cloud model is capable of qualitatively reproducing some familiar aspects of the highly inhomogeneous global cloud distribution. In the free troposphere, clouds are most prevalent in the mid- and high latitudes (especially over the storm tracks), where the cloud fraction often exceeds 20% and extends vertically through almost the entire tropospheric column. The tropical upper troposphere (~100–300 hPa) is another place with large cloud fraction. As a reminder, the model used here does not have parameterized or resolved convection. In the subtropical dry zones cloud fraction is generally less than 10%. The transition from cloud liquid to ice follows the freezing line.

b. *Perturbation experiments*

We use the cloud model to explore how RH and clouds would vary with increased e_s. The results are given in Fig. 7. A uniform increase of 14% barely causes any change in RH (UN minus CNTL-C; Fig. 7, top); WV increases approximately by the same percentage as e_s. The inherent nonlinearity of the Clausius–Clapeyron relation (i.e., the temperature dependence of the fractional increase of e_s per degree of warming) gives rise to appreciable increase of free-tropospheric RH, which amounts to more than 1% in the subtropical dry zones and midlatitude lower troposphere (TS minus CNTL-C; Fig. 7, middle). An attempt to take into account the additional effect of upper-tropospheric and polar warming (TC minus CNTL-C; Fig. 7, bottom) amplifies the same pattern seen in TS.

The corresponding changes in cloud fraction are shown in Fig. 8. There is almost no change in UN (Fig. 8,

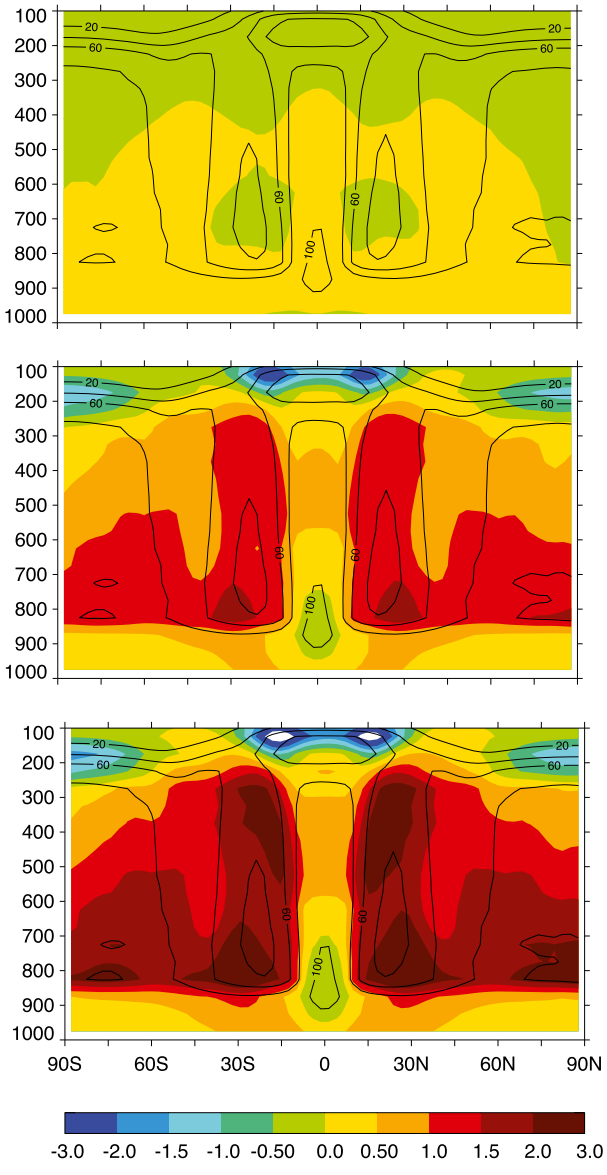

FIG. 7. RH difference (%; color shading) between (top) UN and CNTL-C, (middle) TS and CNTL-C, and (bottom) TC and CNTL-C. The contours with an interval of 20% represent RH in CNTL-C.

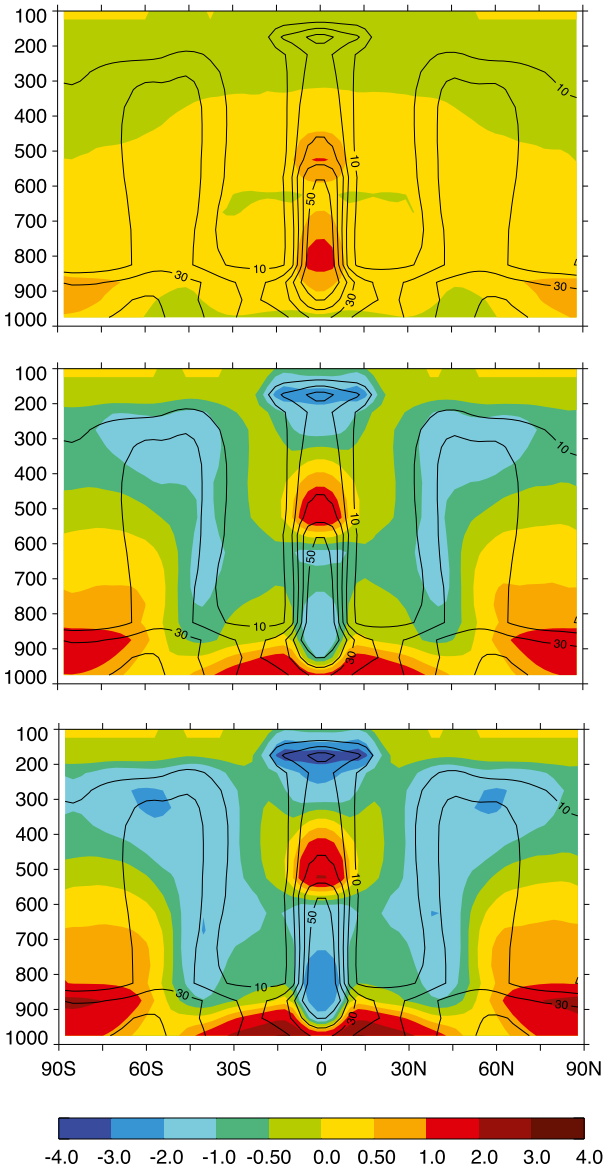

FIG. 8. Cloud fraction difference (%; color shading) between (top) UN and CNTL-C, (middle) TS and CNTL-C, and (bottom) TC and CNTL-C. The contours with an interval of 10% represent the cloud fraction in CNTL-C.

top), consistent with the muted response in RH. Both TS and TC give rise to marked reductions of similar spatial pattern. In TC, cloud fraction decreases by up to 2% in the subtropical dry zones. The entire free troposphere over ~30°–50° also undergoes substantial reduction of cloud fraction (~2%). This trend extends to the high-latitude upper troposphere. The result that cloud fraction decreases despite higher RH is counterintuitive; they typically decrease together in the free extratropical troposphere in comprehensive GCM comparisons (Zelinka et al. 2013). From the perspective of cloud parameterization, the idealized model effectively diagnoses cloud fraction from RH since WV is usually much larger than the cloud condensates.

To better understand the opposing RH and cloud fraction changes, we examine the probability distributions of instantaneous RH and cloud fraction for a domain between 15° and 45°N and between 600 and 700 hPa (Fig. 9). The RH distribution (Fig. 9, top) is reminiscent of that produced with the back trajectory technique [Fig. 6.17 of Pierrehumbert et al. (2007)]. Unlike the specific GCM used in Pierrehumbert et al. (2007), the idealized model, despite having low resolution, simulates a strong dry spike

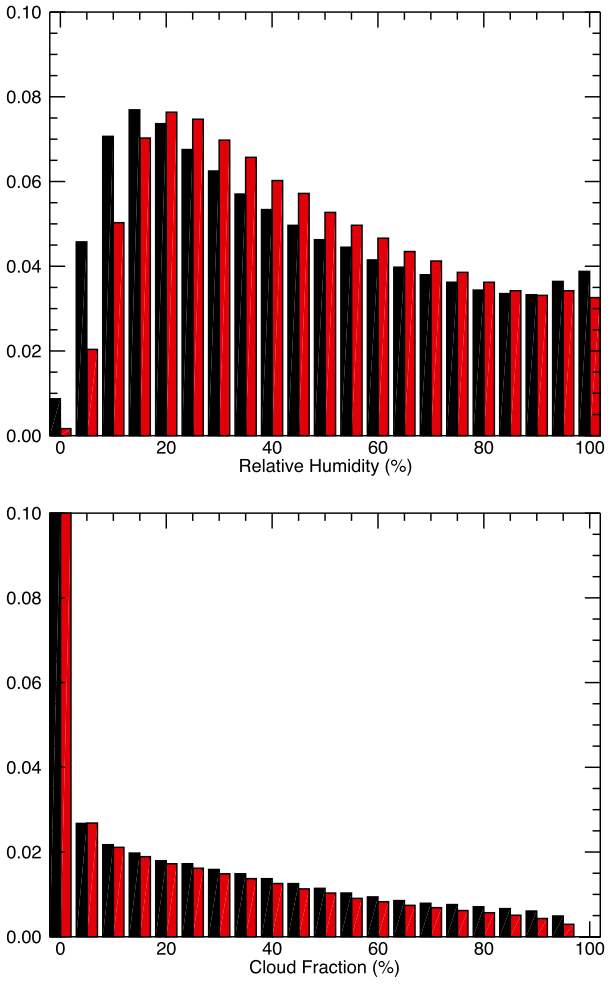

FIG. 9. Normalized histograms of (top) daily RH (%) and (bottom) cloud fraction (%) in a domain between 15° and 45°N and between 600 and 700 hPa. The 20 bins are of equal width (5%). The black and red bars represent CNTL-C and TC, respectively. Note that the y axis in bottom is cut off at 0.1.

in the probability distribution of RH. As RH increases, its occurrence becomes less frequent. Only occasionally does RH rise above 80%, the approximate threshold for cloud formation in the default cloud model. The vast majority of the samples are cloud free (Fig. 9, bottom). The cloud fraction distribution is relatively flat all the way to ~80%, but with a distinct bump between 80% and 100%.

In comparison with CNTL-C, the uneven increase of e_s in TC shifts the dry spike in RH toward higher RH, accompanied by a marked increase in probability of intermediate RH (20%–80%). At the same time, values higher than 80% become less likely. On balance, the former outweighs the latter, resulting in an increase of the average RH. The lower occurrence of RH greater than 80% explains the reduction in the average cloud fraction.

One can rationalize the RH changes using the concept of last saturation (Pierrehumbert et al. 2007). The WV specific humidity q of a descending parcel (with its present temperature denoted as T_1) is the same as the saturated specific humidity q_s when it last experienced saturation (with its temperature denoted as T_0). Thus, its RH at pressure P_1 can be written as $[e_s(T_0)/e_s(T_1)](P_1/P_0)$, where P_0 is the atmospheric pressure of the parcel when it reaches the last saturation. If one imposes the increase of e_s in the form of Eq. (3), the perturbed RH would be $[e_s(T_0)/e_s(T_1)](P_1/P_0)(T_1/T_0)^3$, which is an increase since T_1 is greater than T_0 for a descending parcel. For an ascending parcel, T_0 is greater than T_1, meaning that RH would become smaller with increased e_s if q is conserved. The assumption of constant q does not hold for precipitating parcels once they are saturated, but the fact that T_0 is greater than T_1 for ascending parcels suggests that larger displacements are needed to achieve saturation, resulting in a decrease in RH on average in these ascending parts of the circulation. Parcels drier (wetter) than ~80% RH are typically associated with descending (ascending) motion, and the above analysis helps explain why the dry parcels become more humid in the two perturbation experiments with spatial variations, while the opposite occurs to the wet ones. The latter is the underlying cause of reduced cloud fraction. These simulations are missing the effects of the increase in depth of the troposphere with warming that reduces the increase in the temperature of last saturation and therefore damps the increase in RH that would otherwise occur. It has been shown that both tropical and midlatitude drying can affect subtropical RH (Galewsky et al. 2005; Dessler and Minschwaner 2007). Further analysis is needed to clarify the class of trajectories in this model that are responsible for the reduction in the frequency of high RH values and cloud cover.

The argument above for the reduction of cloudiness in this model should also work in the case of the passive water model with pure saturated adjustment and with no explicit condensate in the sense that there should also be a reduction in the frequency of very high RH values with the change in saturation vapor pressure consistent with the nonuniform warming specified in TC. We have confirmed that this is in fact the case with the saturation adjustment model (Fig. 10).

Cloud liquid and ice respond largely in opposite directions (Figs. 11 and 12, respectively). Despite higher RH in the lower free troposphere, cloud liquid generally decreases with cloud fraction. In contrast, cloud ice increases at higher altitudes, more consistent with RH change. Note that the temperature used for partitioning condensate into liquid and ice does not change; the upward shift of the freezing line, which is often discussed in

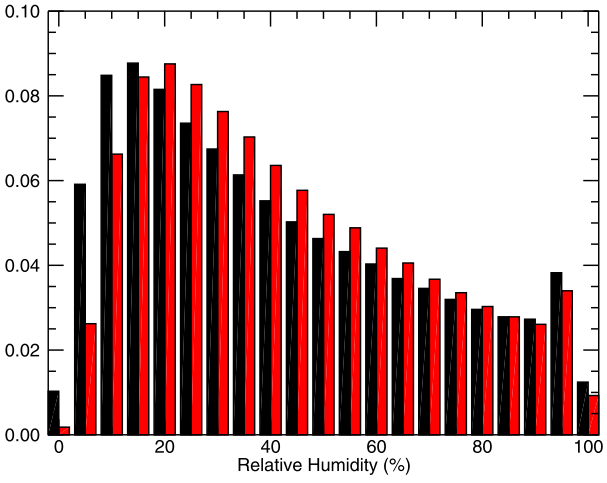

FIG. 10. As in Fig. 9 (top), but for black and red bars representing CNTL-SA (the control simulation of the saturation adjustment model) and a perturbation case analogous to TC, respectively.

the literature, is not an issue here. Thus, it is not straightforward to compare these results with full GCM simulations.

4. Discussion and conclusions

One can think of the idealized model introduced in this paper as a natural extension of the advection–condensation theory/model that was instrumental for understanding the distribution of tropospheric WV. By decoupling WV and clouds from circulation, the model helps answer to what extent they can be rationalized as being driven by a given circulation. The advection–condensation theory makes the case that circulation is the dominant factor in shaping the large-scale structure of RH. Given the strong link between RH and clouds (cloud fraction in particular), one probably should not be surprised by how well the idealized model is able to reproduce some of the salient features of the global cloud distribution. This suggests that it may be feasible to study the climatology of certain cloud systems (e.g., frontal and cirrus clouds) in a noninteractive mode.

A main characteristic of full GCM-simulated response to CO_2-induced warming is a widespread reduction of free-tropospheric cloud fraction equatorward of 60° [Fig. 6 of Zelinka et al. (2013)]. This coincides with a reduction of RH [Fig. 2 of Sherwood et al. (2010)] and is usually attributed to circulation changes (namely the poleward shift of storm tracks and the upward expansion of troposphere). It is interesting that the idealized model, when forced cleanly by a purely thermodynamical effect (namely increased saturated water vapor pressure, one of the most robust outcomes of warming), is able to simulate a similar reduction of cloud fraction in the absence of any circulation change. Even more interestingly, the disappearance of clouds is accompanied by an enhancement of average RH. These results are useful for thinking about full GCM-simulated positive cloud feedback. First, although it is reasonable to expect circulation changes to have certain bearings on cloud distribution at the boundaries of circulation regimes, their roles may be somewhat limited within the interiors as warming-induced circulation changes are generally subtle. Second, average RH is not generally a good proxy for cloud fraction as cloud formation is skewed

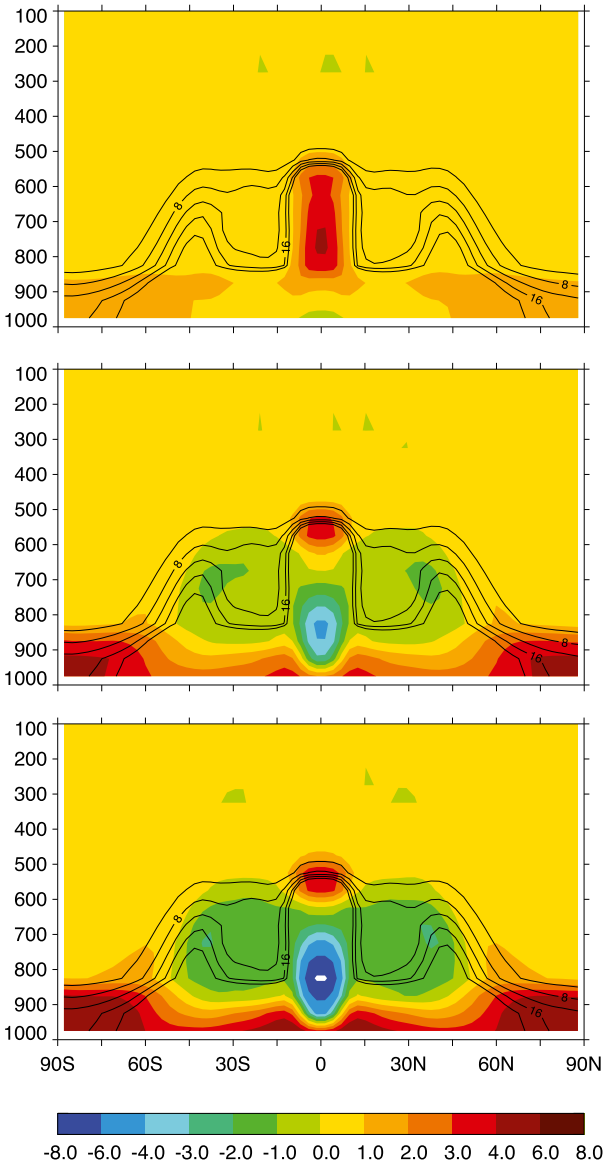

FIG. 11. Cloud liquid difference (10^{-6} kg kg^{-1}; color shading) between (top) UN and CNTL-C, (middle) TS and CNTL-C, and (bottom) TC and CNTL-C. The contours with an interval of 4 × 10^{-6} kg kg^{-1} represent the cloud fraction in CNTL-C.

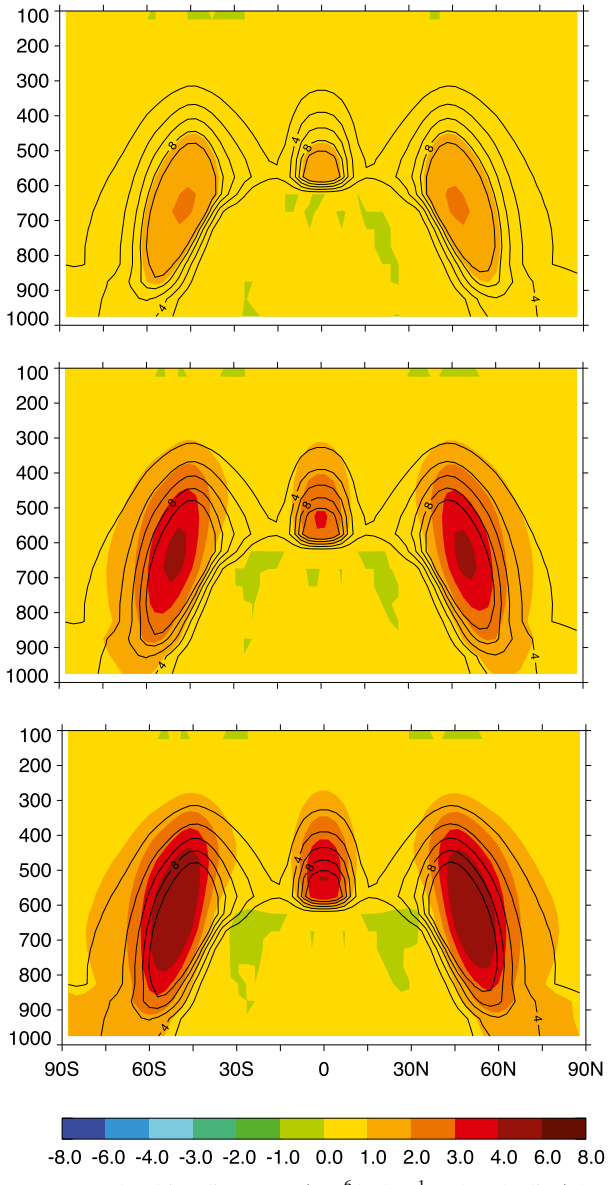

FIG. 12. Cloud ice difference (10^{-6} kg kg^{-1}; color shading) between (top) UN and CNTL-C, (middle) TS and CNTL-C, and (bottom) TC and CNTL-C. The contours with an interval of 2×10^{-6} kg kg^{-1} represent the cloud fraction in CNTL-C.

strongly to high RH. Third, the spatial pattern of warming (e.g., upper-tropospheric and polar amplifications) may be effective at altering the probability distribution of both RH and clouds.

There is an extensive literature on low cloud feedbacks in GCMs, with some recent studies highlighting the roles of convection in affecting tropospheric cloud condensates and WV through convective detrainment (Sherwood et al. 2014; Mauritsen and Stevens 2015; Zhao et al. 2016) in addition to boundary layer processes in isolation (e.g., Zhang et al. 2013). Because the idealized model does not have boundary layer or cumulus parameterization, its utility for studying low cloud feedback and possible connection with convection is limited. More specifically, the mechanism for midlatitude free-tropospheric cloud reduction identified here is different from the thermodynamically induced thinning of boundary layer clouds widely discussed in the literature (e.g., Bretherton and Blossey 2014; Bretherton 2015), despite the fact that both invoke the temperature dependence of saturated water vapor pressure. The former results rather straightforwardly from a reduction in the spatial gradient of saturated water vapor pressure, while the latter is linked to the condensate budget.

One motivation for suggesting a model with passive WV and clouds in a dry dynamical core is to remove the distinctions in cloud simulations that result from differences in convection schemes in GCMs, allowing a focus on the roles of cloud microphysical and macrophysical (cloud fraction) assumptions. Computations with this class of models may also prove useful in isolating dependencies on the resolution and numerics of the dynamical core arising from the presence of a microphysical package.

In conclusion, we present an idealized model that tracks WV and clouds as tracers, but does not allow them to interact with circulation either through latent heat release or CRE. It can simulate many gross features of WV and cloud distributions in extratropical free troposphere. The subtropical dry zones, midlatitude storm tracks, and upper-tropospheric cirrus are captured qualitatively in the simulations. It is found that cloud microphysics (namely rain re-evaporation) plays a modest role in moistening the lower troposphere in this model. An uneven increase of saturated water vapor pressure motivated by global warming simulations has a tendency to reduce free-tropospheric cloud fraction, while RH increases.

Acknowledgments. The authors thank Peter Phillips for help with model setup, and Michelle Frazer for useful discussion. Ming Zhao and Max Popp kindly reviewed an earlier version of the paper.

APPENDIX

Tracer Advection

The dynamical core is a standard spectral core with the prognostic variables vorticity, divergence, temperature, and the logarithm of surface pressure with Simmons–Burridge (Simmons and Burridge 1981) vertical differencing and with all variables, including the

components of the velocities, defined at the same grid points (an A grid) on a latitude–longitude Gaussian grid. Because the logarithm of surface pressure is the prognostic variable, the model does not conserve mass exactly.

Advecting this model's passive tracers, WV and especially the condensed water phases utilized by the microphysics, with spectral advection would contaminate these fields hopelessly with Gibbs' ripples. Instead we use a finite-volume gridpoint advection scheme. We first write the advection operator in an equivalent ''faux flux form'' without weighting the velocity by the pressure thickness (i.e., surface pressure):

$$\mathbf{v} \cdot \nabla \xi = \nabla \cdot (\mathbf{v}\xi) - \xi \nabla \cdot \mathbf{v}. \tag{A1}$$

Note that ξ represents tracer concentration, and $\mathbf{v}$ wind speed. The last term is evaluated on the A grid since the spectral model provides the divergence on this grid. The horizontal faux flux-form transport is computed using the finite-volume formulation of Lin and Rood (this formulation is hereinafter referred to as LR) (Lin and Rood 1996). The velocities are first linearly interpolated to the C grid. The horizontal transport is then evaluated assuming a piecewise linear approximation to the subgrid distribution of tracer, while the vertical transport uses a piecewise parabolic assumption, with monotonicity limiters as in LR. We also evaluate separately the ''integer flux'' contribution to the zonal advection, avoiding any time step constraint due to zonal advection near the poles, once again as in LR. The latter is necessary for an efficient scheme on the latitude–longitude grid.

The spectral model uses leapfrog time step with filtering to avoid separation of even and odd time steps. The tracer advection is adapted to this framework by advecting the tracer over a leapfrog time of $2\delta t$ and using the same Robert filter on the tracer fields.

This way of incorporating gridpoint advection into a spectral model has some awkward features but has advantages in simplicity over other approaches, and shares the problem of nonconservation globally. The quality of this formulation is illustrated by the Polvani and Esler (2007) study of transport of tracers during baroclinic life cycles and the Galewsky et al. (2005) analysis of the sources of subtropical WV, both of which use this algorithm.

Our motivation for retaining a spectral core is the exact zonal symmetry of the algorithm, which is an attractive feature for idealized studies such as this in which the model climate should be exactly zonally symmetric in the absence of sampling errors or the (unlikely) nonuniqueness of the climate state. The circulation in this Held–Suarez idealized dry model has become a standard test of the numerics in GCMs. The sensitivity of the cloud simulation to the numerical implementation of the microphysical package as well as to the tracer advection numerics in the model formulation proposed here may also prove to be of value.

REFERENCES

Anderson, J. L., 2004: The new GFDL global atmosphere and land model AM2–LM2: Evaluation with prescribed SST simulations. *J. Climate*, **17**, 4641–4673, doi:10.1175/JCLI-3223.1.

Blackburn, M., and Coauthors, 2013: The aqua-planet experiment (APE): Control SST simulation. *J. Meteor. Soc. Japan*, **91A**, 17–56, doi:10.2151/jmsj.2013-A02.

Bony, S., and Coauthors, 2015: Clouds, circulation and climate sensitivity. *Nat. Geosci.*, **8**, 261–268, doi:10.1038/ngeo2398.

Bretherton, C. S., 2015: Insights into low-latitude cloud feedbacks from high-resolution models. *Philos. Trans. Roy. Soc.*, **373A**, 20140415, doi:10.1098/rsta.2014.0415.

——, and P. N. Blossey, 2014: Low cloud reduction in a greenhouse-warmed climate: Results from Lagrangian LES of a subtropical marine cloudiness transition. *J. Adv. Model. Earth Syst.*, **6**, 91–114, doi:10.1002/2013MS000250.

Dessler, A. E., and K. Minschwaner, 2007: An analysis of the regulation of tropical tropospheric water vapor. *J. Geophys. Res.*, **112**, D10120, doi:10.1029/2006JD007683.

Donner, L. J., and Coauthors, 2010: The dynamical core, physical parameterizations, and basic simulation characteristics of the atmospheric component of the GFDL global coupled model CM3. *J. Climate*, **24**, 3484–3519, doi:10.1175/2011JCLI3955.1.

Frierson, D. M. W., 2007: The dynamics of idealized convection schemes and their effect on the zonally averaged tropical circulation. *J. Atmos. Sci.*, **64**, 1959–1976, doi:10.1175/JAS3935.1.

——, I. M. Held, and P. Zurita-Gotor, 2006: A gray-radiation aquaplanet moist GCM. Part I: Static stability and eddy scale. *J. Atmos. Sci.*, **63**, 2548–2566, doi:10.1175/JAS3753.1.

Galewsky, J., A. Sobel, and I. M. Held, 2005: Diagnosis of subtropical humidity dynamics using tracers of last saturation. *J. Atmos. Sci.*, **62**, 3353–3367, doi:10.1175/JAS3533.1.

Hartmann, D. L., and K. Larson, 2002: An important constraint on tropical cloud–climate feedback. *Geophys. Res. Lett.*, **29**, 1951, doi:10.1029/2002GL015835.

Held, I. M., 2005: The gap between simulation and understanding in climate modeling. *Bull. Amer. Meteor. Soc.*, **86**, 1609–1614, doi:10.1175/BAMS-86-11-1609.

——, and M. J. Suarez, 1994: A proposal for the intercomparison of the dynamical cores of atmospheric general circulation models. *Bull. Amer. Meteor. Soc.*, **75**, 1825–1830, doi:10.1175/1520-0477(1994)075<1825:APFTIO>2.0.CO;2.

Lin, S.-J., and R. B. Rood, 1996: Multidimensional flux-form semi-Lagrangian transport schemes. *Mon. Wea. Rev.*, **124**, 2046–2070, doi:10.1175/1520-0493(1996)124<2046:MFFSLT>2.0.CO;2.

Mauritsen, T., and B. Stevens, 2015: Missing iris effect as a possible cause of muted hydrological change and high climate sensitivity in models. *Nat. Geosci.*, **8**, 346–351, doi:10.1038/ngeo2414.

O'Gorman, P. A., and T. Schneider, 2008: The hydrological cycle over a wide range of climates simulated with an idealized GCM. *J. Climate*, **21**, 3815–3832, doi:10.1175/2007JCLI2065.1.

Pierrehumbert, R. T., H. Brogniez, and R. Roca, 2007: On the relative humidity of the atmosphere. *The Global Circulation of the Atmosphere*, T. Schneider and A. H. Sobel, Eds., Princeton University Press, 143–185.

Polvani, L. M., and J. G. Esler, 2007: Transport and mixing of chemical air masses in idealized baroclinic life cycles. *J. Geophys. Res.*, **112**, D23102, doi:10.1029/2007JD008555.

Rotstayn, L. D., 1997: A physically based scheme for the treatment of stratiform clouds and precipitation in large-scale models. I: Description and evaluation of microphysical processes. *Quart. J. Roy. Meteor. Soc.*, **123**, 1227–1282, doi:10.1002/qj.49712354106.

——, B. F. Ryan, and J. Katzfey, 2000: A scheme for calculation of the liquid fraction in mixed-phase clouds in large-scale models. *Mon. Wea. Rev.*, **128**, 1070–1088, doi:10.1175/1520-0493(2000)128<1070:ASFCOT>2.0.CO;2.

Salathé, E. P., and D. L. Hartmann, 1997: A trajectory analysis of tropical upper-tropospheric moisture and convection. *J. Climate*, **10**, 2533–2547, doi:10.1175/1520-0442(1997)010<2533:ATAOTU>2.0.CO;2.

Sherwood, S. C., 1996: Maintenance of the free-tropospheric tropical water vapor distribution. Part II: Simulation by large-scale advection. *J. Climate*, **9**, 2919–2934, doi:10.1175/1520-0442(1996)009<2919:MOTFTT>2.0.CO;2.

——, and C. L. Meyer, 2006: The general circulation and robust relative humidity. *J. Climate*, **19**, 6278–6290, doi:10.1175/JCLI3979.1.

——, W. Ingram, Y. Tsushima, M. Satoh, M. Roberts, P. L. Vidale, and P. A. O'Gorman, 2010: Relative humidity changes in a warmer climate. *J. Geophys. Res.*, **115**, D09104, doi:10.1029/2009JD012585.

——, S. Bony, and J.-L. Dufresne, 2014: Spread in model climate sensitivity traced to atmospheric convective mixing. *Nature*, **505**, 37–42, doi:10.1038/nature12829.

Simmons, A. J., and D. M. Burridge, 1981: An energy and angular-momentum conserving vertical finite-difference scheme and hybrid vertical coordinates. *Mon. Wea. Rev.*, **109**, 758–766, doi:10.1175/1520-0493(1981)109<0758:AEAAMC>2.0.CO;2.

Sun, D.-Z., and R. S. Lindzen, 1993: Distribution of tropical tropospheric water vapor. *J. Atmos. Sci.*, **50**, 1643–1660, doi:10.1175/1520-0469(1993)050<1643:DOTTWV>2.0.CO;2.

Tompkins, A. M., 2002: A prognostic parameterization for the subgrid-scale variability of water vapor and clouds in large-scale models and its use to diagnose cloud cover. *J. Atmos. Sci.*, **59**, 1917–1942, doi:10.1175/1520-0469(2002)059<1917:APPFTS>2.0.CO;2.

Wright, J. S., A. H. Sobel, and G. A. Schmidt, 2009: Influence of condensate evaporation on water vapor and its stable isotopes in a GCM. *Geophys. Res. Lett.*, **36**, L12804, doi:10.1029/2009GL038091.

Zelinka, M. D., S. A. Klein, K. E. Taylor, T. Andrews, M. J. Webb, J. M. Gregory, and P. M. Forster, 2013: Contributions of different cloud types to feedbacks and rapid adjustments in CMIP5. *J. Climate*, **26**, 5007–5027, doi:10.1175/JCLI-D-12-00555.1.

Zhang, M., and Coauthors, 2013: CGILS: Results from the first phase of an international project to understand the physical mechanisms of low cloud feedbacks in single column models. *J. Adv. Model. Earth Syst.*, **5**, 826–842, doi:10.1002/2013MS000246.

Zhao, M., I. M. Held, S.-J. Lin, and G. A. Vecchi, 2009: Simulations of global hurricane climatology, interannual variability, and response to global warming using a 50-km resolution GCM. *J. Climate*, **22**, 6653–6678, doi:10.1175/2009JCLI3049.1.

——, and Coauthors, 2016: Uncertainty in model climate sensitivity traced to representations of cumulus precipitation microphysics. *J. Climate*, **29**, 543–560, doi:10.1175/JCLI-D-15-0191.1.